Building and Environment 205 (2021) 108224

Contents lists available at ScienceDirect

Building and Environment

journal homepage: www.elsevier.com/locate/buildenv

Spatiotemporal impact of vehicle heat on urban thermal environment: A case study in Hong Kong

Xuan Chen [a], Jiachuan Yang [a,*], Rui Zhu [b], Man Sing Wong [b], Chao Ren [c]

[a] Department of Civil and Environmental Engineering, The Hong Kong University of Science and Technology, Hong Kong, China
[b] Department of Land Surveying and Geo-Informatics, The Hong Kong Polytechnic University, Hong Kong, China
[c] Faculty of Architecture, The University of Hong Kong, Hong Kong, China

ARTICLE INFO

Keywords:
Anthropogenic heat
Vehicle heat
Urban heat island
Urban morphology
WRF simulation

ABSTRACT

Vehicle heat (VH) is a substantial portion of anthropogenic heat and can affect the urban thermal environment. Quantifying the impact of VH has implications for the potential benefits of electric vehicles in cities, yet the spatiotemporal impact of VH has not been investigated separately. This study incorporates VH and urban landscape data into the Weather Research and Forecasting (WRF) model to estimate the VH impacts at a fine spatial resolution over Hong Kong. Results show a strong temporal variation of the VH impact at daily, weekly, and seasonal scales: 1) the warmth of urban canyon air temperature is stronger and more consistent at night than in daytime, 2) increases in sensible heat fluxes are more pronounced during weekdays than weekends, 3) temperature change of 0.35 °C in winter is larger than that of 0.32 °C in summer. Increased air temperature over the land area by VH correlates with urban area fraction and building height positively, but not the aspect ratio. The statistically significant VH impact (90% confidence level) has the broadest spatial coverage in Hong Kong shortly after rush hours. The relative VH impact compared to building heat demonstrates the dominative role of vehicle heat in warming low urbanized areas with highways and circulation roads. The spatiotemporal distributions of the VH impact provide insights into the potential benefits of green transportation technology and policy in mitigating urban heat islands.

1. Introduction

Anthropogenic heat (AH) and land cover modification are two main contributors to the higher temperature in cities, a phenomenon called the urban heat island (UHI). Although cities only cover less than 5% of the earth surface, they accommodate 55% of the world's population and are responsible for 70% of global energy demand [1,2]. Concentrated release of AH in this small percentage of the earth surface thus has adverse impacts on global human health and energy sustainability [3,4]. Building heat emission, vehicle waste heat and metabolic heat from people are the three main components of AH. The release of AH is spatially varied over different urban land uses, generally being larger in industrial and commercial areas, or/and along the highways/freeways [5–7]. The temporal variation of AH is also evident [8]: daily peaks coincide with morning and evening rush hour periods, and the cold season tends to have a larger emission than the warm season in mid/-high latitude cities. Based on the inventory approach, studies have estimated the emission amount of AH for major cities around the world [9–11]. In recent year, increased data availability allows the estimation of AH emissions at fine spatiotemporal resolutions. For example, Iamarino et al. [12] estimated the AH emissions for London at a resolution of 30 min and 200 × 200 m^2, and Chow et al. [13] produced hourly AH data with a 1 × 1 km^2 resolution for Phoenix, US.

As an additional energy source in the urban environment, AH can modify the intensity and variability of urban heat island [14], aggravate/alleviate the thermal discomfort under heat/cold waves [15,16], and affect the pollution dispersion and urban rainfall pattern [17]. Thus, quantifying the impact of AH on urban climate is as important as estimating the emission amount. The topic has been investigated through numerical weather simulations in the literature. Block et al. [18] found that a 20 W m^{-2} AH could rise the air temperature by 0.5 °C in the populated Ruhr region of Germany, Fan & Sailor [19] reported that the AH release in winter could rise the nighttime air temperature by 2–3 °C in Philadelphia, and Yang et al. [24] suggested that the AH release increased urban air temperature by around 1 °C in the Yangtze River Delta region of China. The AH-induced modification of urban climate

* Corresponding author.
E-mail address: cejcyang@ust.hk (J. Yang).

https://doi.org/10.1016/j.buildenv.2021.108224
Received 28 April 2021; Received in revised form 31 July 2021; Accepted 2 August 2021
Available online 4 August 2021

has substantial seasonal variations. Chen et al. [6] found the AH contributed 65% of the UHI intensity in winter and 17% in summer over the Chinese city Hangzhou.

It is noteworthy that many studies have focused on the effect of aggregated AH, and the impact of individual components of AH has been less explored. Vehicle heat (VH) is generally recognized as the second-largest portion of the AH [11,21], but its separate impact on urban climate has been rarely investigated. For instance, VH contributes 47% of the AH in São Paulo, Brazil [22], and is the major source of AH during summer in France [23]. Moreover, VH is released in the traffic flow associated with residents' commuting pattern, and consequently the spatiotemporal distribution of VH release has great influences on residents' exposure to thermal discomfort [65]. There have been a few studies on the impact of VH. Zhu et al. [25] estimated hourly gridded VH profiles in Hong Kong and found a robust correlation between VH and UHI intensity. They suggested the VH could be a critical driver for UHI at locations surrounded by high-rise buildings, with dense vehicle flows, and at the seaside. Singh et al. [26] integrated hourly spatial VH data into regional climate simulations and estimated the impact of VH over Singapore during April 2016. They found that VH increased the air temperature by 1.1 °C during the morning peak period. However, the study used a mean VH profile for the entire simulation period that the differences between weekday and weekend is neglected. Until now, the spatial and temporal variations of the VH impact on the thermal environment over diverse urban landscapes still remain unclear.

The number of global vehicles has increased from about 670 million in 1996 to 1.32 billion in 2016. And the transportation sector accounts for the largest portion of total greenhouse gas emissions in U.S. For mitigation and adaptation to global warming, governments have encouraged the adoption of high energy-efficient electric vehicles (EV) as a measure to reduce greenhouse gas emissions in the past decade [27]. Global EV stock has reached 7.2 million in 2019 and the EV adoption is accelerating in Europe and Asia [28]. By fully or partly replacing internal combustion engines with electric motors, transformation to electric vehicles can markedly cut waste heat from traffic in cities [29]. Promoting electric vehicles thus has potentials to reduce urban heat islands and benefit the urban thermal environment. To quantify such environmental benefits of EV, it is imperative to estimate the spatiotemporal impact of VH on the urban thermal environment.

In the present study, we choose Hong Kong as an example to investigate the spatiotemporal impact of vehicle heat on urban thermal environment. Hong Kong is a dense Asian city with a population of around 7.4 million and more than 900 thousand vehicles. Due to its high development level, Hong Kong experiences an intense UHI phenomenon and a multitude of associated challenges [30]. Substantial research efforts have devoted to urban climate studies in Hong Kong as a typical test case [31–33]. Fast-increasing car ownership is a severe problem in Hong Kong and the government has implemented policies to promote the use of electric vehicles since 1994. This study aims to quantify the spatial variation of VH impact on the thermal environment over diverse urban landscape, and the temporal variation of VH impact at multiple time scales (daily, weekly and seasonal) in Hong Kong. Towards this end, the study integrated fine-resolution urban canyon parameters [34], building heat data based on the local climate zone map [35], and gridded vehicle heat data [25] into numerical weather simulations. The relationship between the impact of vehicle heat and urban morphological parameters is analyzed, and the relative impact of vehicle heat compared to building heat is assessed.

2. Methodology

2.1. High-resolution numerical weather simulation

The Weather Research and Forecasting (WRF) model version 3.8.1 [36] coupled with a single-layer urban canopy model (SLUCM [37–39], was adopted for performing weather simulations in this study. WRF-SLUCM is one of the most commonly used models applied for urban climate studies, and its accuracy has been extensively evaluated at major cities worldwide [20,40]. Four one-way nested domains were generated with horizontal grid resolutions of 13.5 km (d01; mesh size of 180 × 180), 4.5 km (d02; mesh size of 271 × 271), 1.5 km (d03; mesh size of 301 × 301), and 500 m (d04; mesh size of 409 × 409) (Fig. 1a). The innermost domain (d04) was centred at Hong Kong and covered the entire Greater Bay Area (Fig. 1b). The vertical grid contained 35 full sigma levels from the surface up to 50 hPa. The physical parameterization schemes were chosen as follows: (1) the WSM 6-class graupel scheme for microphysics [41]; (2) the Dudhia [42] and RRTM scheme [43] for shortwave and longwave radiation, respectively; (3) the Eta similarity scheme [44] for the surface layer; (4) the Yonsei University planetary boundary layer scheme [45]; and (5) the Noah LSM scheme [46] for the land surface process over natural land cover. The initial and boundary meteorological conditions were derived from the 6-hourly Global Final Analysis data of the National Center for Environmental Prediction at a 1 ° × 1 ° resolution (http://rda.ucar.edu/datasets/ds083.2/). The United States Geological Survey (USGS) land cover classification data with 28 categories were used to describe the land use land cover over the studied area.

In the default WRF simulations, the land use condition of each grid is determined by the dominant land cover type. A grid is considered as an urban grid when the fraction of urban land use exceeds that of other individual land use types. The SLUCM model is called to solve heat and moisture budgets only over urban grids. To better represent the land use condition, despite the dominant land cover type, we turned on the SLUCM for all grids with an impervious surface fraction larger than zero. The urban portion was solved by the SLUCM, and the non-urban portion was set as the original land use type according to the USGS map and was modelled using the Noah LSM scheme. The WRF simulations adopt a tile approach and estimate the meteorological variables over urban grids by weighted averaging the urban and non-urban areas. Take the sensible heat flux over an urban grid (SH_{grid}) for example,

$$SH_{grid} = SH^{urb} \times FRC + SH^{rul} \times (1 - FRC), \quad (1)$$

where FRC is the urban area fraction of the grid, and superscript urb and rul denote urban and rural areas, respectively. The waste heat by vehicles was assumed to be released in the urban portion of each grid (i.e., added to SH^{urb}).

2.2. Urban canopy parameter

To better represent the heterogeneous urban landscape, we incorporated the urban canopy parameters (UCPs) into the WRF simulations based on the 2016 local climate zone (LCZ) map in this study. The LCZ map was developed using an improved method of the World Urban Database and Portal Tool (WUDAPT) and its overall accuracy reaches 76% [47]. A set of urban canopy parameters, including mean building height, street width, building width, standard deviation of building height, plan area fraction and urban area fraction, was specified for each urban local climate zone. The resolution of the LCZ map is 100 m × 100 m. To be consistent with the grid resolution in WRF d04 (500 m × 500 m), the values of UCPs in each WRF d04 grid was equal to the average of the nearest 25 LCZ grids. Fig. 2 shows the spatial distribution of the urban canopy parameters used in the WRF simulations.

2.3. Vehicle heat data

Hourly gridded vehicle heat data in Hong Kong for weekdays, Saturday, and Sunday at 800 m × 800 m resolution were adopted from Zhu et al. [25]. The data were estimated based on the annual traffic census data of year 2015 from the Transport Department of Hong Kong. Assuming that all the vehicles follow the shortest paths from their origins to the destinations, a cell-transmission-model was developed to

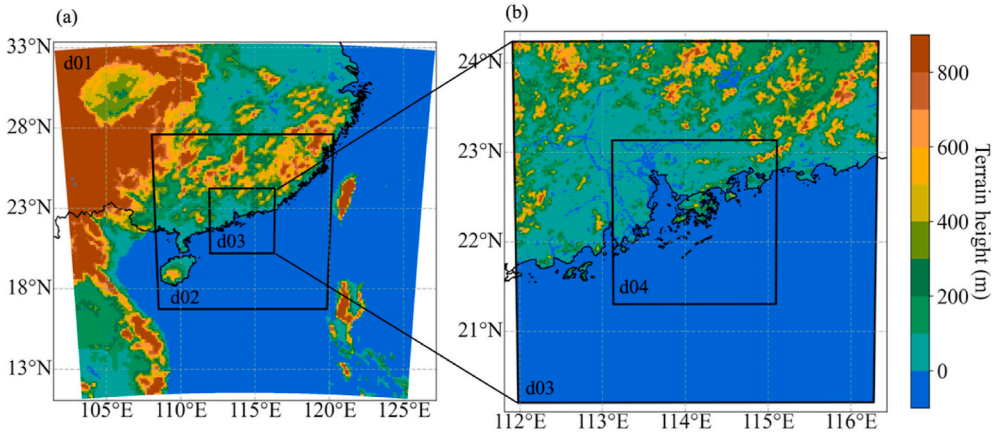

Fig. 1. Nested domain configuration for WRF simulations with a horizontal grid spacing of (a) 13.5 km (d01), 4.5 km (d02), 1.5 km (d03), and (b) 0.5 km (d04) overlaid with the terrain height. The study area Hong Kong is at the center of the innermost domain (d04).

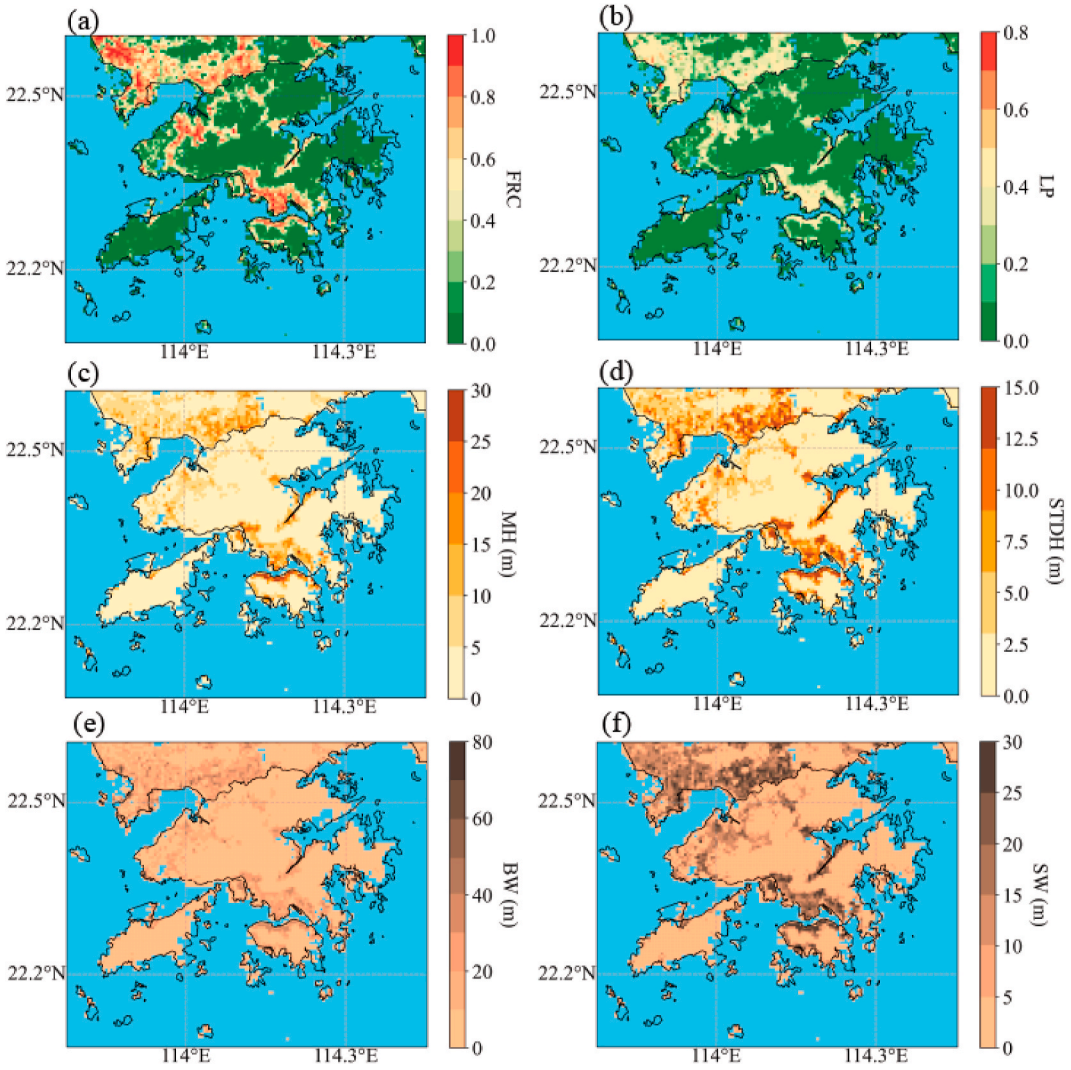

Fig. 2. Spatial distribution of (a) urban area fraction (FRC), (b) mean building height (MH), (c) street width (SW), (d) plan area fraction (LP), (e) standard deviation of building height (STDH), and (f) building width (BW) over Hong Kong.

simulate the vehicular flow over the whole Hong Kong [25]. The correlation coefficient between estimated and measured number of vehicles for all traffic counting stations is higher than 0.8. Three different fuel types of vehicles were considered, and the net heat combustion values were 46.4, 42.8, and 50.2 $\times$ 10^6 J/kg for petrol, diesel, and liquefied petroleum gas. Combining with the travel length of vehicles (m), the ratio of different vehicle types, and the fuel consumption per travel length (kg/m), the accumulated heat emission (J) of vehicular flow was

calculated at an hourly basis. The heat emission was then divided by the time and the grid size to obtain the vehicle heat flux with a unit of W m^{-2} (see Eq. (11)–13 in Ref. [25]. We resampled the original vehicle heat data (800 m × 800 m resolution) to match the innermost WRF domain (d04, 500 m × 500 m resolution) by linear interpolation. In the end, at each grid in d04, a unique VH profile with 3 (weekday, Saturday, and Sunday) × 24 values was inputted to the SLUCM as a part of the sensible heat flux (see Eq. (1)).

Fig. 3a shows the spatial distribution of weekly mean VH (time-averaged VH over one weekly cycle) over Hong Kong. The grids with

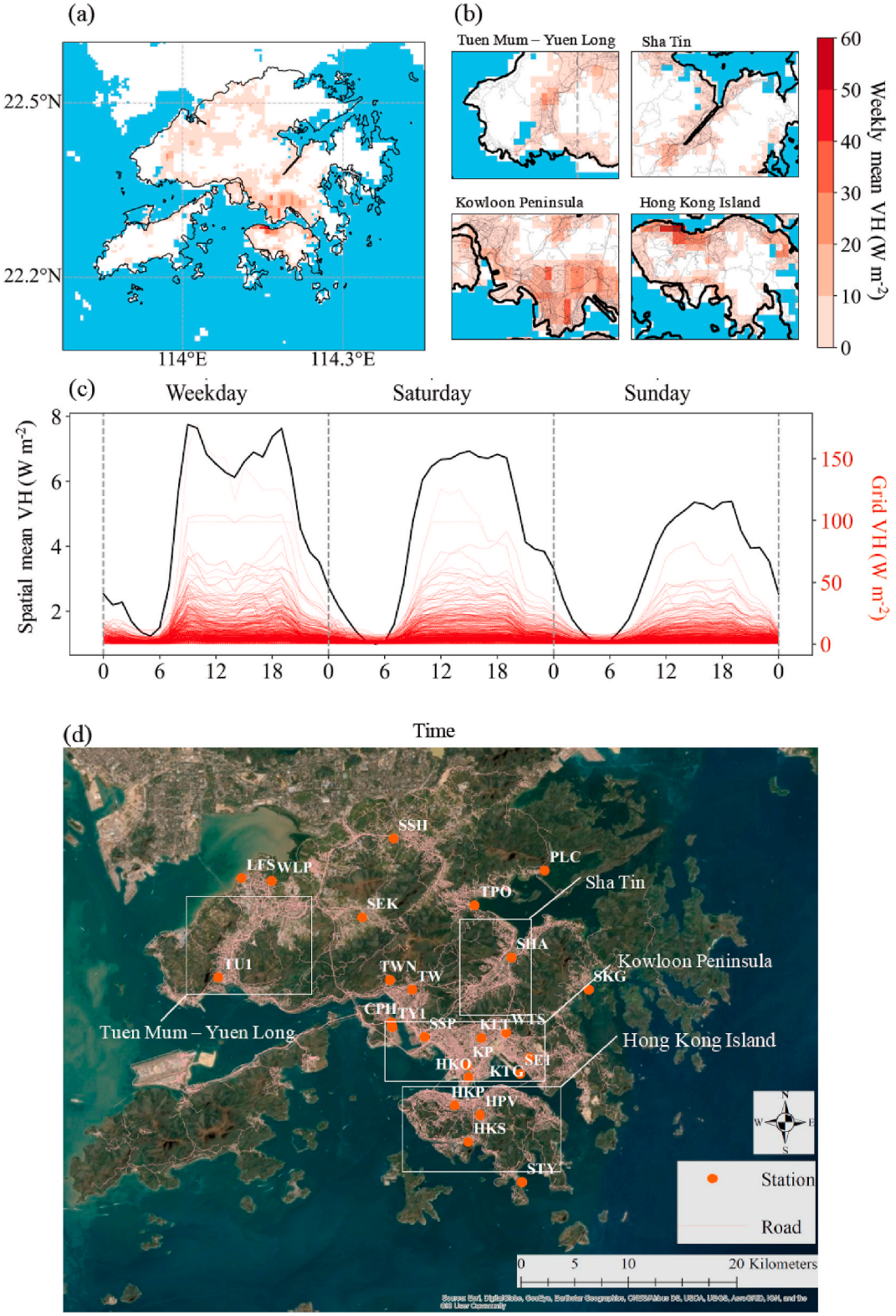

Fig. 3. Spatial distribution of the weekly mean VH over (a) Hong Kong and (b) four core districts; (c) Temporal profile of VH in individual grids (red, right axis) and the spatial mean VH profile (black, left axis); (d) Road network of Hong Kong and the location of weather stations used in this study. (For interpretation of the references to color in this figure legend, the reader is referred to the Web version of this article.)

high VH values were mainly concentrated at four core districts with dense road networks, as shown in Fig. 3b. Fig. 3c shows the temporal profile of VH in all grids (red line, right axis). Despite a large variation in the magnitude, the temporal evolution of VH at different grids is found to be similar. Averaging over the entire land area of Hong Kong, the spatial-mean VH (black line, left axis in Fig. 3c) has a maximum magnitude about 8 W m^{-2} on weekday and about 5 W m^{-2} on Sunday. Two peaks at 9 a.m. and 7 p.m. local time were distinct on weekdays but were not significant on weekends, which were synchronized with the work day and off day human activities. The VH release pattern was consistent with the road network in Hong Kong, which is shown in Fig. 3d.

2.4. Numerical experiments

Numerical experiments were carried out for July (summer) and January (winter) 2015 to investigate the seasonal variation of the VH impact on the urban thermal environment. To accurately estimate the VH impact, spatial variation of building waste heat needs to be considered given its important contribution to the urban thermal environment. Unfortunately, hourly gridded building heat emission data over Hong Kong are not available. To account for the spatial variation of building heat emission, here we adopted a local climate zone based approach [35,48]. A different peak value of building heat emission was assigned to each urban local climate zone, which is consistent with the method used for incorporation of UCPs in section 2.2. Note that the range of anthropogenic heat in the original LCZ classification consists of building waste heat, vehicle heat, and human metabolic heat (Table-4 in Ref. [35]. We cannot directly compute the building heat emission (BH) by subtracting VH from AH, as the underlying methods and assumptions for AH and VH estimations are different. The medium value of the range was used in this study to represent the BH over different urban neighbourhoods, and it varied from 175 W m^{-2} in compact high-rise areas to 5 W m^{-2} in sparsely built areas. The default diurnal profile in the SLUCM was used for estimating the intra-daily variation of BH at all urban grids. The accuracy and representativeness of the default anthropogenic heat profile has been widely evaluated in international cities [10].

Three simulation scenarios were considered in summer: 1) a reference case (NoAH) without anthropogenic heat, 2) a case (BH) with the LCZ based building heat emission, and 3) a vehicle heat case (VH) with building heat and vehicle heat. Because of the sub-tropical climate of Hong Kong, building waste heat is not important in winter [49]. We conducted only two simulations in winter: a reference case (NoAH) without anthropogenic heat and a vehicle heat case (VH) with vehicle heat. The impact of the VH can be represented by the comparison of the BH case and VH case in summer, and by the comparison of the NoAH case and VH case in winter. The simulation periods were from 1st July 00:00 (UTC) to 15th July 00:00 (UTC) and from 1st January 00:00 (UTC) to 15th January 00:00 (UTC). The first day was treated as the spin-up time, and the subsequent analyses focused on 4 weeks, from 2nd July (Thursday) to 15th July (Wednesday) in summer and from 2nd January (Friday) to 15th January (Saturday) in winter.

2.5. Evaluation of weather simulation

The hourly air temperature of year 2015 was collected from 24 ground-based weather stations of the Hong Kong Observatory. All stations have data quality check and the amount of missing data is <5%. The location and ID of the stations are shown in Fig. 3d. The accuracy of WRF-simulated air temperature (T_2) was evaluated through comparisons against the measured air temperature at these stations. Statistical indicators, including root mean square error (RMSE), mean bias error (MBE) and mean absolute error (MAE) were calculated as below:

$$\mathrm{RMSE} = \sqrt{\frac{1}{\mathrm{N}}\sum_{n=1}^{\mathrm{N}}(P_n - O_n)^2}, \tag{2}$$

$$\mathrm{MBE} = \frac{1}{N}\sum_{\mathrm{n}=1}^{\mathrm{N}}(P_n - O_n), \tag{3}$$

$$\mathrm{MAE} = \left|\frac{1}{N}\sum_{\mathrm{n}=1}^{\mathrm{N}}(P_n - O_n)\right|, \tag{4}$$

whereP_n is the predicted value from the WRF simulations and O_n is the observed value, n represents each time step and N is the total time step.

2.6. Revised scheme for canyon air temperature

One important objective of this study is to quantify the VH impact on air temperature inside street canyons. However, the standard canyon air temperature outputted by SLUCM was calculated from the surface temperatures of the road and the walls, which acted as an effective skin temperature of the urban canyon. This method did not directly link canyon air temperature with the anthropogenic heat. Here we adopted a revised scheme proposed by Theeuwes et al. [50] to compute the canyon air temperature to ensure a meaningful VH impact estimation. The new canyon air temperature (T_2^{urb}) considers the heat exchange between the urban canyon and the overlying atmosphere, and the stability condition in the canyon:

$$T_2^{urb} = T_a + \frac{SH_c r_{ah}}{\rho C_p}, \tag{5}$$

where T_a is the air temperature at the lowest atmospheric level, SH_c is the sensible heat flux from the urban canyon to the overlying atmosphere, r_{ah} is the aerodynamic resistance, ρ is the air density, and C_p is the specific heat capacity of dry air. Note that estimated T_2^{urb} from this revised scheme is sensitive to the friction velocity because of the dependence of r_{ah} on stability conditon. During the winter simulation period with extremely strong winds, the scheme could predict unreasonable air temperatures at night. The abnormal values nevertheless compose less than 1% of the simulated temperature data over Hong Kong and were excluded in subsequent analysis.

2.7. Significance test

Due to the inherent uncertainty of regional climate simulations, significance testing is an essential process for ensuring the high possibility of the differences in simulated urban canyon air temperature (T_2^{urb}) between reference cases and the VH case. The significance test allows the investigation of locations that are likely to experience a warmer environment due to VH throughout the simulation period. Here we adopted the T-test at the 0.1 level (90% significance level) to check the significance of the temperature changes. The diurnal cycle (24 h) was separated into eight time periods: 8 a.m.–10 a.m., 11 a.m.–1 p.m., 2 p.m.–4 p.m., 5 p.m.–7 p.m., 8 p.m.–10 p.m., 11 p.m.–1 a.m., 2 a.m.–4 a.m., and 5 a.m.–7 a.m. Each time period contained 42 temperature data (3 h per day during the two-week simulation) in summer and winter, respectively. One significance test was carried out to check the temperature difference induced by VH for each time period separately, and the test covered all grids over the innermost domain d04.

3. Results and discussion

3.1. Model evaluation

Fig. 4 shows the temporal evaluation results for WRF-simulated T_2 in July and January. The hourly values of the root mean square error

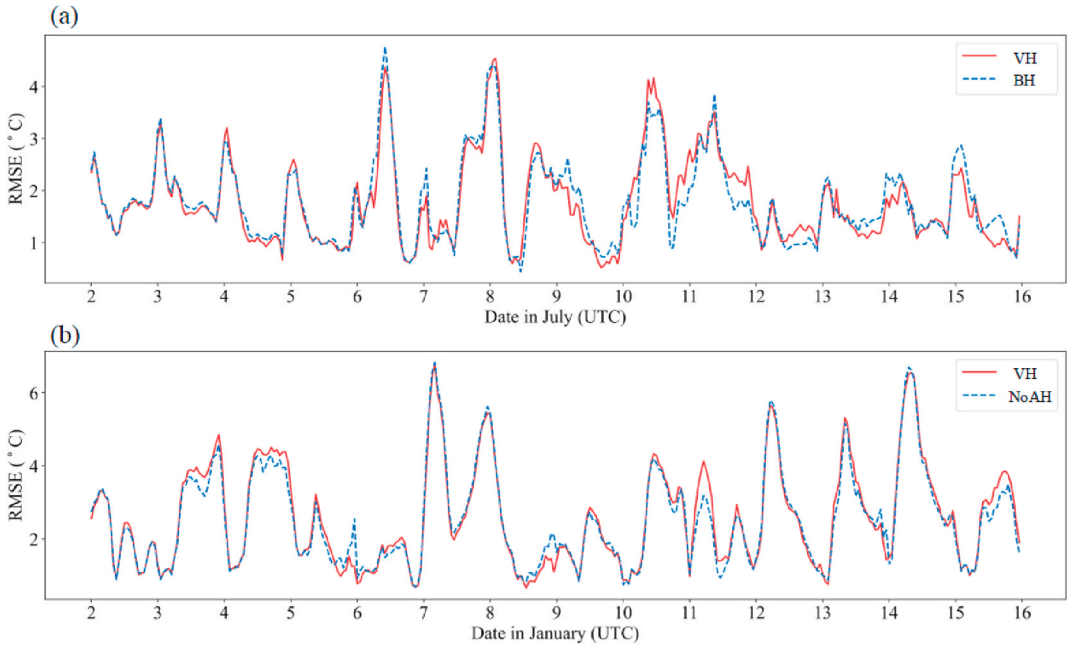

Fig. 4. Temporal variation of mean root mean square error (RMSE) for simulated 2-m air temperature over Hong Kong in (a) summer and (b) winter.

(RMSE) shown in Fig. 4 are the average of the RMSE values at 24 stations (see Fig. 3d) over Hong Kong. The RMSE is smaller in summer than in winter. The mean RMSE for T_2 during the whole study period is 1.79 °C for the BH case and 1.73 °C for the VH case in summer, which increases to 2.54 °C and 2.58 °C in winter, respectively. The results suggest that a detailed VH profile cannot substantially improve the overall simulation accuracy of air temperatures over Hong Kong. One reason is that about one-third of the meteorological stations used for model evaluation locate far away from major roads and are subject to negligible VH impacts. The underestimation of warm-season temperature and overestimation of cold season temperature is partially due to the limitation of the Yonsei University (YSU) planetary boundary layer scheme [51]. Large model errors (>3 °C) are observed on rainy days in summer (results not shown here). The overall RMSE is nevertheless comparable with previous studies, and thus the accuracy of the numerical weather simulations in this study is acceptable. For example, Wang et al. [52] reported a RMSE of about 1.5 °C at 2 weather stations during their 3-days simulations over Hong Kong. Yu et al. [7] found an average RMSE of 3.5 °C for WRF simulations over 67 urban stations in Beijing. One reason for the large model error in winter is the systematic bias of urban canopy models in

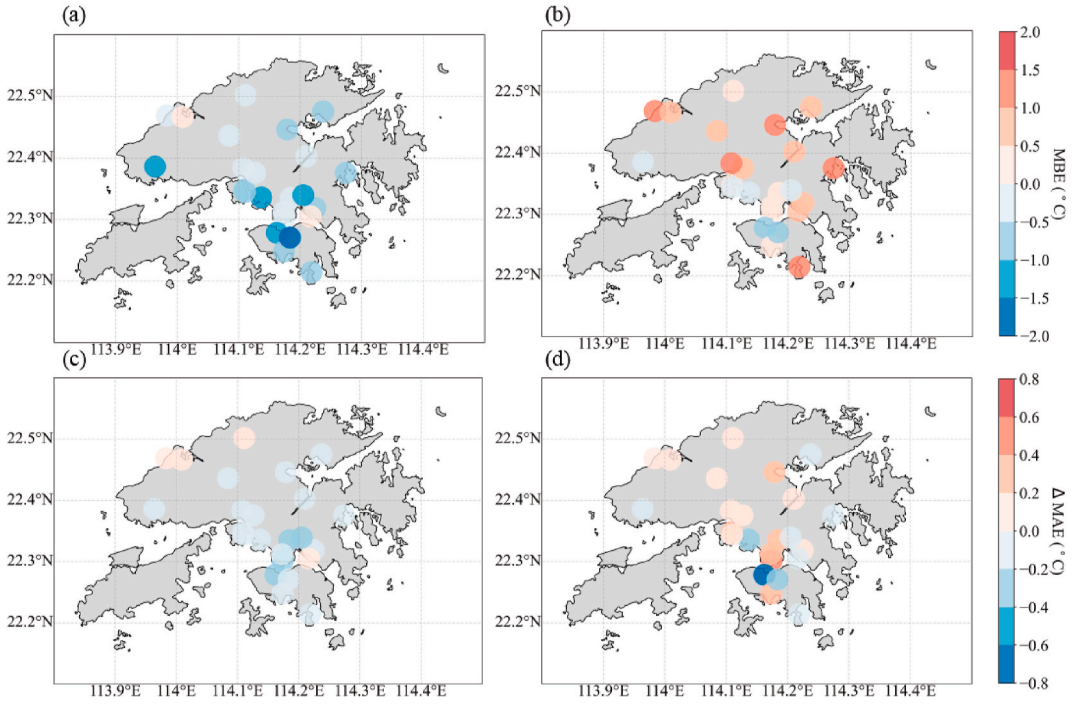

Fig. 5. Temporal average error of simulated T_2 at individual weather stations: (a) mean bias error (MBE) of the BH case in summer, (b) MBE of the NoAH case in winter, (c) differences of the mean absolute error ($\Delta MAE = MAE_{VH} - MAE_{BH}$) in summer, (d) differences of the mean absolute error ($\Delta MAE = MAE_{VH} - MAE_{NoAH}$) in winter.

simulating near surface urban wind speed [53]. The parametrization of urban surface roughness requires improvements for a better usage of the refined canopy parameters in microclimate simulations [54].

Fig. 5a–b shows the temporal average values of MBE in the BH case for individual weather stations in summer and in the NoAH case for winter, respectively. The negative values in blue indicate a model underestimation, and the positive values in red represent a model overestimation. WRF simulations tend to underestimate T_2 in summer (Fig. 5a), and the average MBE for all stations is around −0.46 °C. This underestimation is more evident in the highly urbanized area, with the temporal mean MBE of more than −1.82 °C for HKV, and about −1.10 °C for SSP, WTS and HKP stations located in areas with large urban area fractions (Fig. 3d). The MBE value tends to be larger in the low urbanized areas during winter, and the mean MBE for all stations is 0.64 °C. Only two stations located near compact high-rise regions, HPV and HKP stations, have MBE values reach −1.0 °C. The result is consistent with previous findings that WRF simulations tend to overestimate rural temperatures and underestimate urban temperatures [55,56]. Fig. 5c–d shows the differences of mean absolute error (ΔMAE) between the VH and BH cases for summer, and between the VH and NoAH cases for winter. As the MAE represents the deviation of the simulated temperature from the observations, negative ΔMAE values indicate improved T_2 simulations after incorporating VH profiles. During summer, implementing the VH profile improves the model accuracy at 16 stations out of 24, which are concentrated in highly urbanized areas (Fig. 5c). During the winter, however, adding the VH profile only improves the simulation accuracy at 9 stations. The temporal mean MBE values in present study for all stations nevertheless are between −2 and 2 °C. The error is consistent with recent high-resolution WRF-UCM simulations that incorporate detailed urban canopy parameters: Molnár et al. [64] reported a MBE range of −0.5 – 2 °C in Szeged, Hungary; Yu et al. [53] found a MBE range of -4 – 6 °C in Beijing, China. Our simulation bias indicates a reasonable overall accuracy of the WRF simulations.

3.2. Temporal variation of VH impact

To study the temporal variation of the impact of vehicle heat during weekdays, Saturday and Sunday, we check the difference in the urban sensible heat flux (ΔSH^{urb}) and urban canyon air temperature (ΔT_2^{urb}) between the VH and BH cases in summer, and between the VH and NoAH cases in winter. To reduce the noise introduced by small perturbations in the climate simulations, for each time step, we only include grids with VH values larger than 5 W m^{-2} into the analysis. In Hong Kong, the daytime starts at 6 a.m. and ends at 7 p.m. in summer, and it begins at 7 a.m. and ends at 6 p.m. in winter. Fig. 6a and b shows the impact of VH on ΔSH^{urb} in summer and winter, separately. ΔSH^{urb} is larger in the daytime, especially around or after the rush hours. The standard deviation of ΔSH^{urb} during daytime is found to be larger than that during nighttime. In terms of the seasonal variation, the mean ΔSH^{urb} for the 2-week simulation period is 26.45 W m^{-2} during summer and 22.79 W m^{-2} during winter. And it is clear that the summer standard deviations are larger than the winter ones. Summer weather in Hong Kong is more unstable than winter weather, with heavy precipitation, strong monsoon, and notable land-sea breeze [57,58]. The changes in regional atmospheric forcing disturb the urban climate and contribute to the large variation of VH impact in summer.

By modifying sensible heat fluxes, VH releases lead to changes in urban canyon air temperature (Fig. 6c and d). After adding VH profiles, WRF-simulated 2-week mean T_2^{urb} increases by 0.32 °C in summer and by 0.35 °C in winter over the VH emission area. Although ΔSH^{urb} by vehicle heat is larger in summer, the mean and standard deviation of ΔT_2^{urb} are larger in winter than in summer. One important reason is that the same amount of VH becomes a larger fraction of the total sensible heat flux during winter as the natural radiation level decreases [19]. Another plausible reason could be the strong land-sea breezes during summer, which spread VH from the releasing points to surrounding areas quickly [49,58]. And the VH impact becomes uniform in summer with a smaller standard deviation due to the spreading. The strongest VH impact occurs at noontime during weekdays in summer and the spatial mean ΔT_2^{urb} reaches 0.5 °C. Despite the positive VH, negative values of ΔT_2^{urb} could occur at weekends during winter daytime, especially on Sundays with low traffic flow and small VH. Results here demonstrate that the VH impact varies with time notably at the daily scale, weekly scale, and seasonal scale. It is worth mentioning that the temporal analysis in this section only includes areas with considerable VH emission (i.e., >5 W m^{-2}). The time series results only illustrate partial effects of VH, as VH could also modify surrounding rural areas. Thus, spatial analysis with significance test is conducted next to investigate the spatial variation of VH impact.

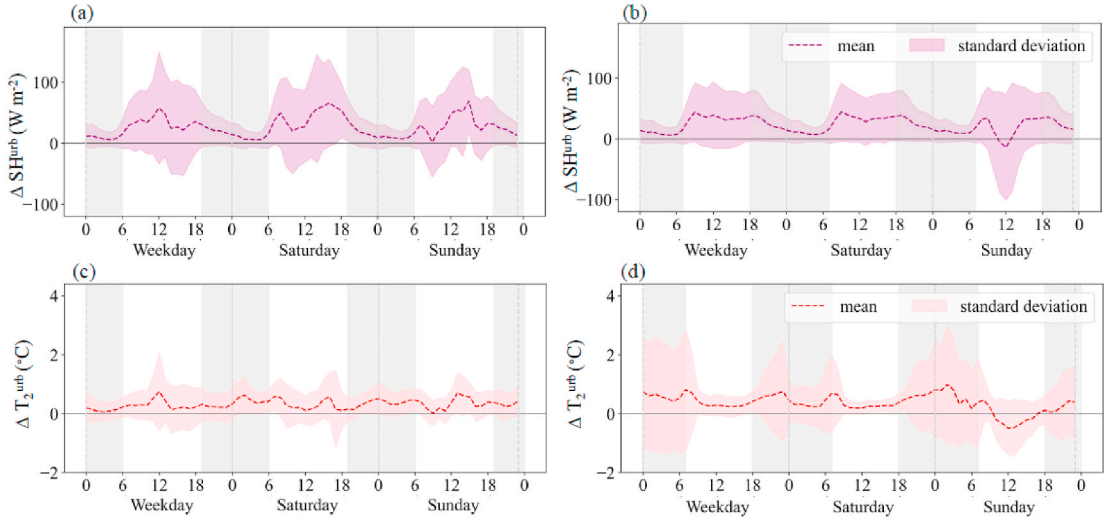

Fig. 6. Differences of (a) SH^{urb} between the VH and BH cases in summer, (b) SH^{urb} between the VH and NoAH cases in winter, (c) T_2^{urb} between the VH and BH cases in summer, and (d) T_2^{urb} between the VH and NoAH cases in winter. The dash lines represent the mean differences and the shaded areas represent one standard deviation away from the mean. The grey (white) color represents the nighttime (daytime) period. (For interpretation of the references to color in this figure legend, the reader is referred to the Web version of this article.)

3.3. Spatial variation of VH impact

Fig. 7 shows the spatial distribution of ΔT_2^{urb} over Hong Kong in summer. Results at different time periods throughout the diurnal cycle are presented. VH emissions increase T_2^{urb} over most land areas (positive ΔT_2^{urb}) during all the time periods in summer. From 8 a.m. to 10 a.m. (Figs. 7a), 92% of the Hong Kong land area experiences a higher urban canyon air temperature, with a spatial mean of 0.12 °C. At late night from 11 a.m. to 1 p.m., VH increases mean urban canyon air temperature of the land area by 0.3 °C (Fig. 7b). Although lower ΔT_2^{urb} is shown during the afternoon, the maximum ΔT_2^{urb} can reach about 1.5 °C in summer daytime. The VH impact becomes weaker at summer nights due to the weak VH emission, with a mean ΔT_2^{urb} around 0.1 °C during 2 a.m.–4 a.m. The dotted areas in Fig. 7 represent regions where VH-induced temperature changes are statistically significant at the 90% confidence level. The largest spatial mean ΔT_2^{urb} by VH is found during the morning rush hours (8 a.m.–10 a.m.) (Fig. 7a), with a spatial mean of 0.84 °C over the significant grids (11 km^2). The strongest VH impact of a single grid can be up to 1.57 °C during 8 p.m.–10 p.m. (Fig. 7e). The areas with a significant VH impact have the largest spatial extent from

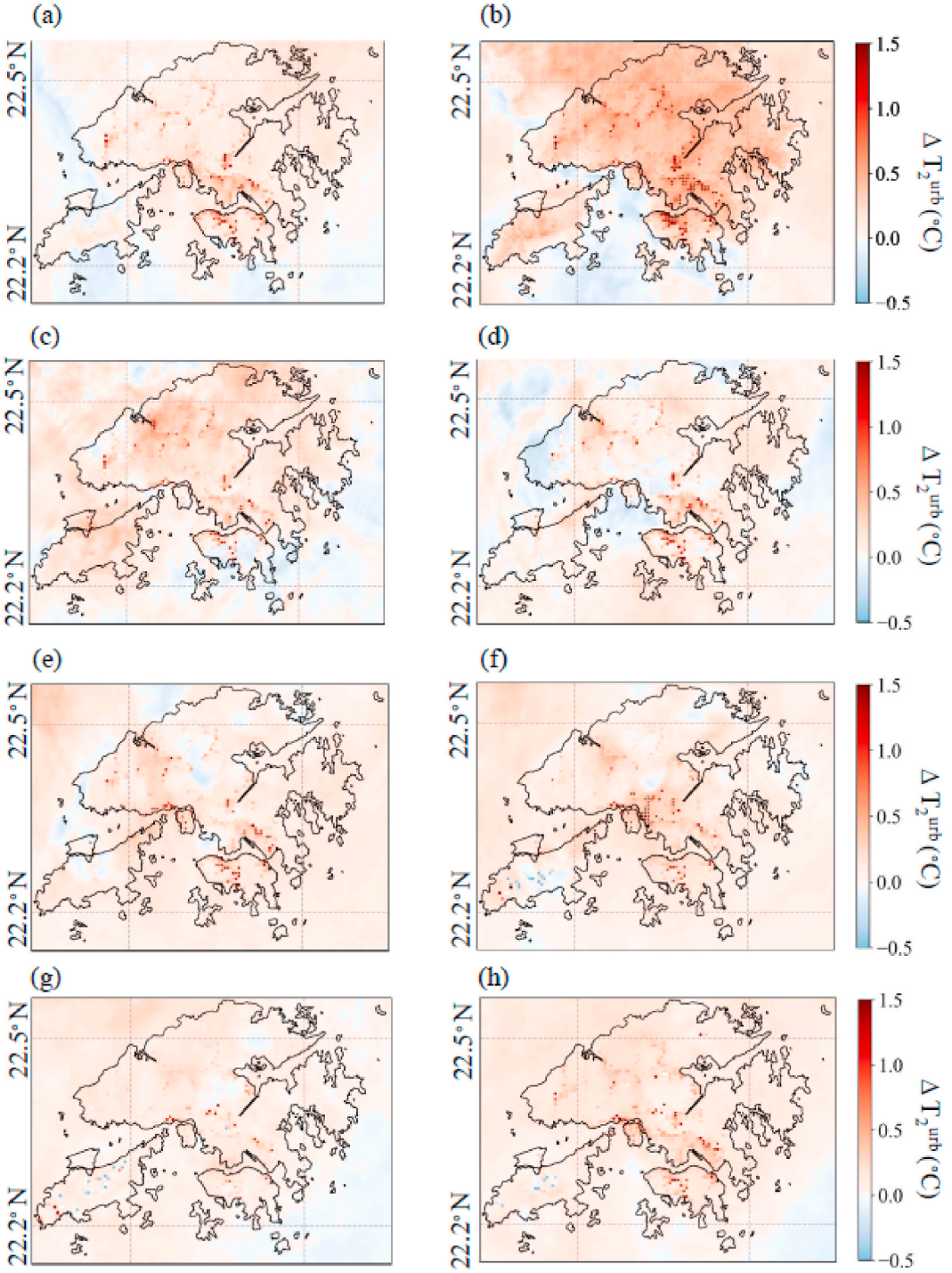

Fig. 7. Spatial distribution of the mean difference in ΔT_2^{urb} between the VH and BH cases over Hong Kong in summer: (a) 8 a.m.–10am, (b) 11 a.m.–1 p.m., (c) 2 p.m.–4 p.m., (d) 5 p.m.–7 p.m., (e) 8 p.m.–10 p.m., (f) 11 p.m.–1 a.m., (g) 2 a.m.–4 a.m., (h) 5 a.m. – 7am. Dotted areas stand for regions with impacts statistically significant at the 0.1 level.

11 a.m. to 1 p.m. in summer, covering a total of 38 km^2 land area.

The VH impact on urban canyon air temperature is more noticeable and concentrated around the road network in winter (Fig. 8). This is consistent with the temporal results shown in Fig. 6. During the winter morning and afternoon rush hours (Fig. 8a and d), around 67% of the land area experiences increased T_2^{urb} by VH. The ΔT_2^{urb} is also strong during nighttime (Fig. 8e and f) over four core distrcits. The largest spatial mean ΔT_2^{urb} of 0.16 °C occurs during 11 p.m.–1 a.m. Strong VH impact is also found over the low-density urban area with highways in the northern part of Hong Kong during 8 p.m.–1 a.m. This proves that where VH is the only contributor of the anthropogenic heat, it can be a major factor for the nighttime warming at neighbourhoods with large traffic flow. In winter, the spatial mean ΔT_2^{urb} over the significant grids (dotted areas in Fig. 8) is greater than 1.00 °C at different periods throughout the day. Between 8 p.m. and 10 p.m., a total of 38.25 km^2 land area has significantly higher temperature caused by VH and the mean ΔT_2^{urb} is 1.08 °C. Note that the significant VH impact on T_2^{urb} has the widest spatial coverage usually on the periods after the rush hours.

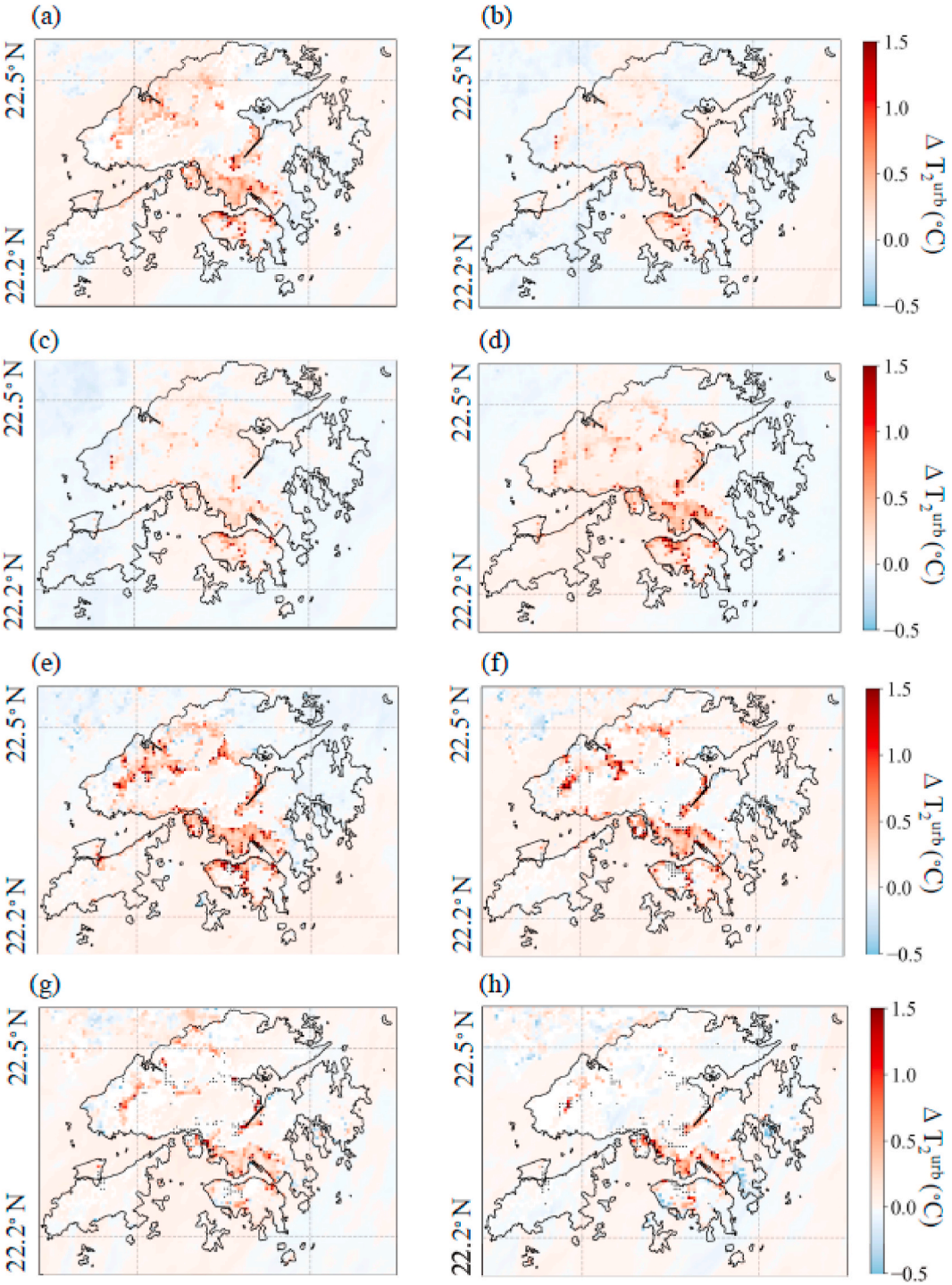

Fig. 8. Spatial distribution of the mean difference in ΔT_2^{urb} between the VH and NoAH cases over Hong Kong in winter: (a) 8 a.m.–10am, (b) 11 a.m.–1 p.m., (c) 2 p.m.–4 p.m., (d) 5 p.m.–7 p.m., (e) 8 p.m.–10 p.m., (f) 11 p.m.–1 a.m., (g) 2 a.m.–4 a.m., (h) 5 a.m. – 7am. Dotted areas stand for regions with impacts statistically significant at the 0.1 level.

This may be caused by the spread of strong VH releases to nearby areas.

3.4. Relationship between VH impact and urban morphology

To diagnose the VH impact on the thermal environment in different urban neighbourhoods, we examine the relationship between the VH impact and urban morphology in this section. Fig. 9 shows the distribution of ΔT_2^{urb} over different ranges of three urban morphology parameters (urban area fraction, mean building height, and the aspect ratio) during one daytime period (8 a.m.–10 a.m.) and one nighttime period (11 p.m.–1 a.m.) in summer. A general increasing trend is found between ΔT_2^{urb} and FRC, and between ΔT_2^{urb} and MH for the entire land area. For highly urbanized regions with 0.8–1.0 FRC, mean ΔT_2^{urb} is around 0.20 °C in the morning (Fig. 9a) and around 0.10 °C at night (Fig. 9b). Neighbourhoods with tall buildings (>24 m) have 0.21 °C higher ΔT_2^{urb} than those with 0–6 m buildings during morning time in summer (Fig. 9b). The highest ΔT_2^{urb} is found over the tall buildings area at nighttime (Fig. 9c). Note that the box plots exclude the outliers that the maximum values are slightly different in the results of different morphology parameters for the same period. The distributions of ΔT_2^{urb} over significant grids are different from those over the whole land area in Hong Kong. The significant ΔT_2^{urb} means the area has a high possibility to experience a warmer environment throughout the whole study period due to VH. During the morning rush hours, most of the grids with significant ΔT_2^{urb} belong to the lowest FRC group (0–0.2). The mean significant ΔT_2^{urb} reaches 0.86 °C (Fig. 9a) in the morning and 0.65 °C (Fig. 9b) at night. A similar pattern is found in the distribution over the mean building height. The highest significant ΔT_2^{urb} belongs to the lowest MH group (0–6 m) in summer. On the other hand, VH-induced ΔT_2^{urb} over entire land area and over significant grids do not have a clear relationship with the aspect ratio (Fig. 9e and f). The maximum significant ΔT_2^{urb} is found over neighbourhoods with a MH/SW of 0.6–0.8 in summer.

Positive relationships between ΔT_2^{urb} and FRC/MH over the entire land area are also found in winter. Compared to the summer results, the relationships are more obvious at winter nights. Mean ΔT_2^{urb} is about 0.1 °C in regions with FRC of 0–0.2 and about 0.29 °C in regions with FRC of 0.8–1.0 during the morning rush hour (Fig. 10a). Neighbourhoods with tall buildings (>24 m) experience the strongest VH impact, with a mean ΔT_2^{urb} of 0.62 °C at night between 11 p.m. and 1 a.m. Similar to summer time, the relationship between aspect ratio and ΔT_2^{urb} is unclear. The magnitude of VH and urban morphology jointly influence the urban thermal environment. Tall buildings reduce the air ventilation and subsequent dispersion of anthropogenic heat that high-rise neighbourhoods can strengthen urban nighttime warming, as pointed out in previous studies [49,59]. Meanwhile, vehicle heat emission depends on the traffic density on roads that wide streets tend to have notable VH emissions. This is one reason that ΔT_2^{urb} has a strong relationship with the mean building height but not with the aspect ratio over entire land area. In terms of the distributions over the significant grids, patterns between ΔT_2^{urb} and FRC/MH on winter nights are different from those on summer nights. During winter nights, highly urbanized areas with FRC of 0.6–1.0 have a mean ΔT_2^{urb} around 1.19 °C. With respect to the relationship with mean building height, ΔT_2^{urb} is prominent in neighbourhoods with the lowest and highest buildings. The mean significant ΔT_2^{urb} is 1.13 °C for the 0–6 m MH group and is 1.24 °C for the >24 m MH group (Fig. 10d). The major reason is that the VH is released along the roads, and many highways and city circulation roads with large traffic flow are located in low urbanized areas in Hong Kong, such as along the seashore or near mountains. On the top of this, part of highly urbanized neighbourhoods or/and high-rise building area are downtown regions with dense traffic, where the VH can be trapped among the buildings. During winter nights, the impact of VH on urban thermal environment becomes more noticeable and leads to the largest mean significant ΔT_2^{urb} among studied periods.

3.5. Comparison of VH and building heat impacts

Results in sections 3.2–3.4 show the absolute magnitude of the VH impact on urban canyon air temperature, here we compared the VH

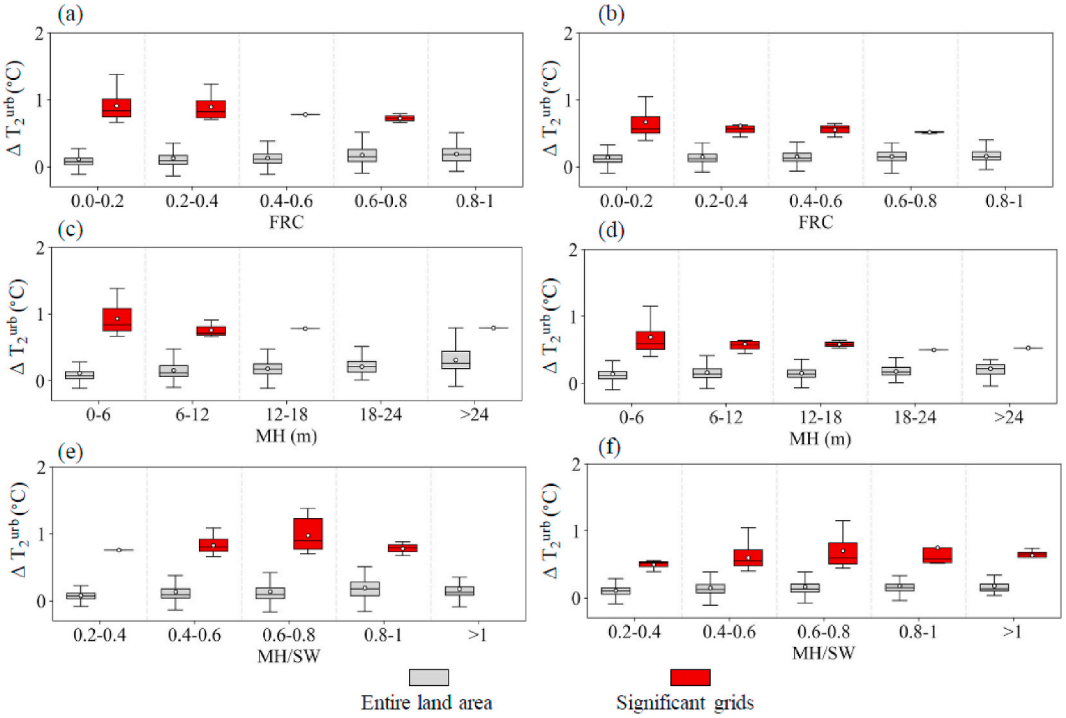

Fig. 9. Distribution of ΔT_2^{urb} over different ranges of (a) and (b) urban area fraction (FRC), (c) and (d) mean building height (MH), (e) and (f) the aspect ratio (MH/SW) during (left) 8 a.m.–10 a.m. and (right) 11 p.m.–1 a.m. in summer. Significant grids denote the areas with vehicle heat impact statistically significant at the 90% confidence level.

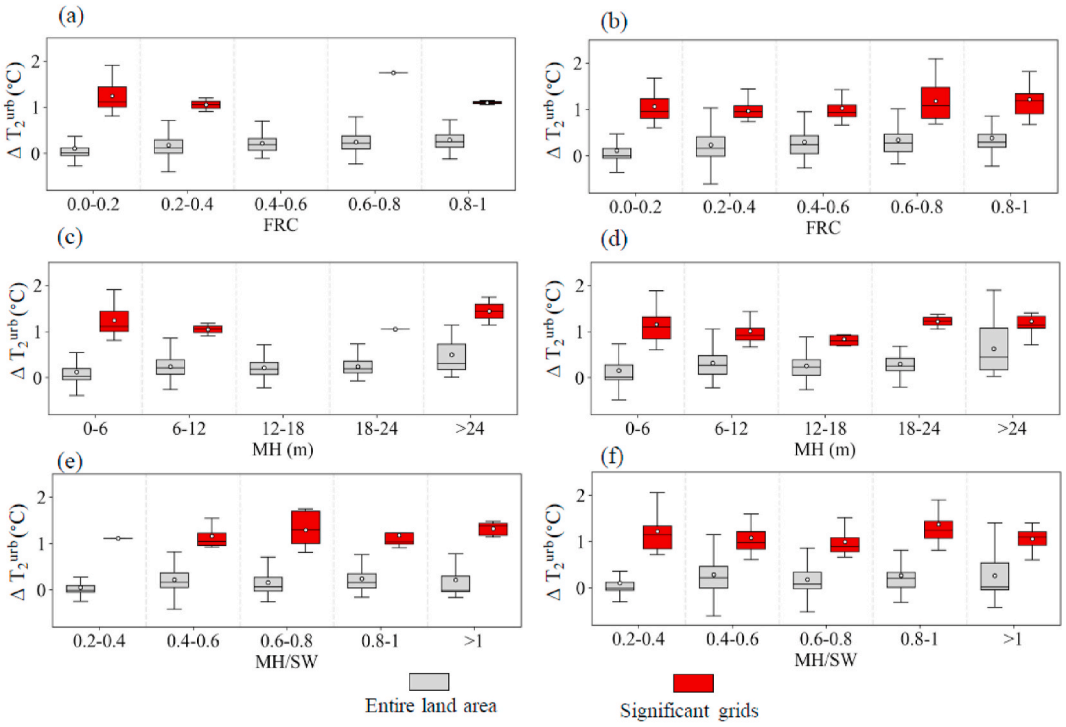

Fig. 10. Distribution of ΔT_2^{urb} over different ranges of (a) and (b) urban area fraction (FRC), (c) and (d) mean building height (MH), (e) and (f) the aspect ratio (MH/SW) during (left) 8 a.m.–10 a.m. and (right) 11 p.m.–1 a.m. in winter. Significant grids denote the areas with vehicle heat impact statistically significant at the 90% confidence level.

impact against the building heat (BH) impact to provide insight into the relative contribution of vehicle heat to the thermal environment over different neighborhoods in summer. The VH impact was estimated as the ΔT_2^{urb} between the VH and BH cases, while the BH impact was computed as the ΔT_2^{urb} between the BH and NoAH cases (see section 2.4). Fig. 11 shows the relationship between ΔT_2^{urb} and three urban morphology parameters over entire land area and over the grids with significant VH impacts separately. Over the entire land area, the total ΔT_2^{urb} under the combined effect of VH and BH increases with FRC and MH in the morning and at night. This indicates a hotter thermal environment in more urbanized regions. The increase of total ΔT_2^{urb} is mainly caused by BH that the relative contribution of VH decreases from 45% (40%) to 31% (25%) as the FRC (MH) increases in the morning. Similar trends are observed at night. Over the areas with significant VH impact, VH synergistically interact with building waste heat that ΔT_2^{urb} can reach over 1.5 °C. Vehicle heat contributes more than 80% of the total ΔT_2^{urb} in open canyons with MH/SW of 0.2–0.4, and about 50% of the total ΔT_2^{urb} in compact neighborhoods with MH/SW of 0.8–1. The BH impact on canyon air temperature also tends to be more evident over the areas with significant VH impact. The interaction between VH and BH is nevertheless complex that BH-induced ΔT_2^{urb} reduces over the neighbourhood with FRC of 0.2–0.4 in the morning, and the neighbourhoods with MH of 12–24 m at night. Findings here complement the results of the absolute impact of VH in summer. Vehicle heat dominates over building heat in regulating the urban thermal environment only over a small portion of Hong Kong land area. Nevertheless, the warming effect of VH is so strong in these areas that total ΔT_2^{urb} can be three times larger than the mean ΔT_2^{urb} by anthropogenic heat over the whole Hong Kong.

4. Conclusion

In this paper, we quantify the spatiotemporal effect of vehicle heat on the thermal environment of Hong Kong using the coupled WRF-SLUCM modelling system. Results show that VH emissions have a more substantial impact on the urban canyon air temperature (T_2^{urb}) during weekdays than over weekends. Strong seasonal variations of the VH impact are found, where VH impact is stronger and more concentrated near the road network in winter. Simulated 2-week mean T_2^{urb} increases by 0.35 °C in winter and by 0.32 °C in summer over the VH emission area. The VH impact on the thermal environment has large spatial variations, and negative temperature changes can be found over some land areas during the daytime due to the inherent uncertainty of climate simulations. Yet, highly urbanized regions in Hong Kong consistently experience a warmer thermal environment by vehicle heat, especially around the rush hours and at night. At the 90% significance level, the statistically significant VH impact on T_2^{urb} has the widest spatial extent shortly after the rush hours. Over the whole land area in Hong Kong, it is found that VH impact increases with urban area fraction and mean building height. However, the areas with statistically significant VH impacts are mainly low urbanized regions with large traffic flows and highly urbanized regions with tall buildings. In these regions, VH impact on urban thermal environment is comparable or greater than the building waste heat effect. The joint influence of VH and BH drastically elevates the air temperature in compact neighbourhoods, where urban heat mitigation is urgently needed.

It is noteworthy that with a focus on vehicle heat impact, the representation of building heat and other AH components is largely simplified in this study. Modelling building waste heat in urban climate simulations nevertheless requires the development of building energy parameterizations for the single-layer urban canopy model, which is beyond the scope of this study. One limitation of the present study is that the impact of VH is only investigated through canyon air temperature. The humidity and wind speed can also be affected by the VH. Previous studies pointed out that AH can dry the built environment [56,60], and modify the potential temperature profiles in the planetary boundary layer [17]. Future studies may explore the impact of vehicle heat on a variety of microclimatic variables in diverse urban neighbourhoods. It should also be emphasized that the SLUCM in this study treats the urban canopy as a single layer, and the VH impact on air temperature at

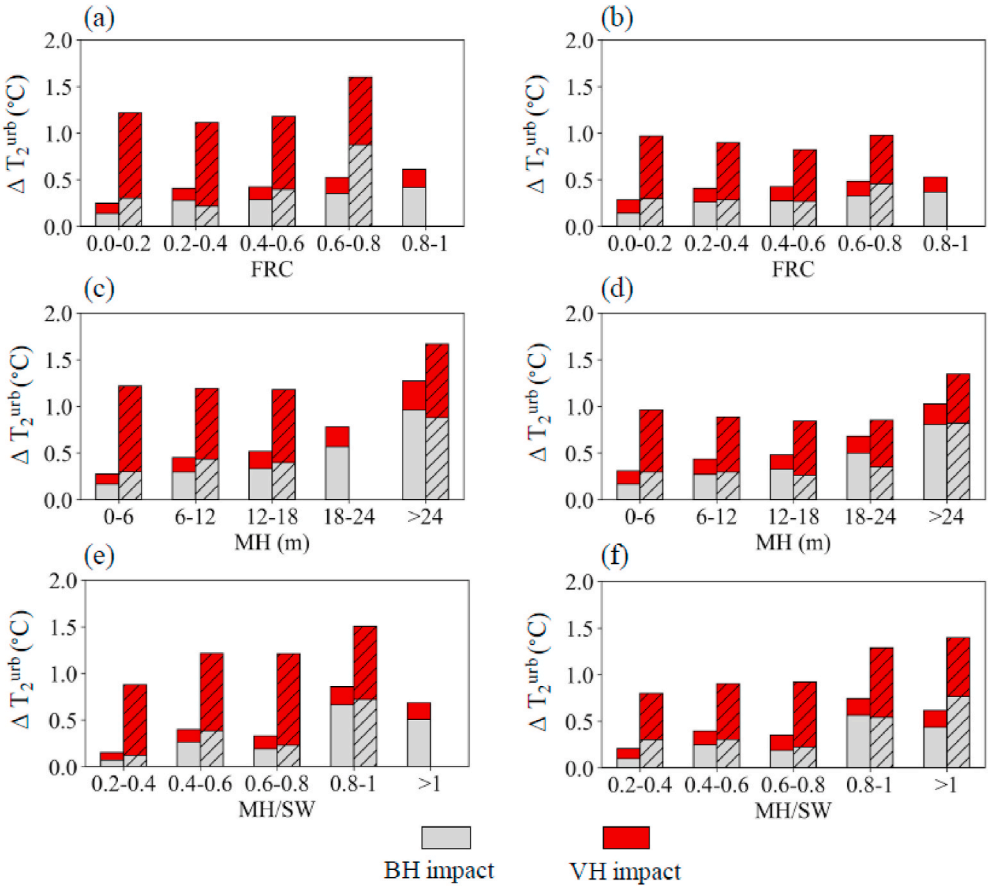

Fig. 11. Relative impact of vehicle heat to building heat on ΔT_2^{urb} over different ranges of (a) and (b) urban area fraction (FRC); (c) and (d) mean building height (MH); (e) and (f) the aspect ratio (MH/SW) during (left) 8 a.m.–10 a.m. and (right) 11 p.m.–1 a.m. in summer. Clear bars are results over the entire land area, and shaded bars denote the results over areas with vehicle heat impact statistically significant at the 90% confidence level.

different heights inside the street canyon can not be examined. To quantify the VH impact at the neighbourhood scale with detailed configurations of the urban landscape, vertical discretization is necessary and multi-layer urban canopy models shall be adopted [40].

A higher urban canyon air temperature due to the VH could increase the population exposure to heat stress in Hong Kong, especially around rush hours and evenings. The VH impact has implications for population health risk, and transportation policies should take such implications into consideration. Until 2020, Hong Kong has more than 18000 electric vehicles, reaching to about 2% of the total vehicle amount [61]. The Hong Kong government plans to double the number of charging facilities to promote the EV [62]. Although the primary goal of the EV promotion is to achieve the carbon neutrality for Hong Kong by 2050, results of this study demonstrate the environmental benefit of the EV in enhancing the thermal environment during summer. Because of the positive feedback between the air temperature and energy demands [63], potential benefits in energy saving by reducing the VH can be of interests in future studies. Our study provides a good estimation of the VH impact on air temperature in one of the most densely populated cities. Quantifying the impact of vehicle heat is important for other large metropolitan areas worldwide given the global trend of electrifying vehicles [26,27]. Urban datasets are becoming readily accessible through government platforms in recent years, including but not limited to building morphology, traffic, demography, and energy usage. By integrating urban datasets into numerical weather simulations, the obtained high-resolution map can provide useful information for climate-related urban policy. The methodology adopted in this study can be easily applied for other cities to study the vehicle heat impact and potential benefit of electric vehicles.

Declaration of competing interest

The authors declare that they have no known competing financial interests or personal relationships that could have appeared to influence the work reported in this paper.

Acknowledgements

This work was supported by the Hong Kong Research Grants Council funded project 26202319. The numerical simulation for this article was supported by the supercomputer services at the National Tianhe-2 Center in Guangzhou, P.R. China.

References

[1] E.J. Gago, J. Roldan, R. Pacheco-Torres, J. Ordóñez, The city and urban heat islands: a review of strategies to mitigate adverse effects, Renew. Sustain. Energy Rev. 25 (2013) 749–758, https://doi.org/10.1016/j.rser.2013.05.057.
[2] United Nations, Revision of World Urbanization Prospects, Department of Economic and Social Affairs, 2018.
[3] A. Salvati, H. Coch Roura, C. Cecere, Assessing the urban heat island and its energy impact on residential buildings in Mediterranean climate: barcelona case study, Energy Build. 146 (2017) 38–54.
[4] M. Santamouris, N. Papanikolaou, I. Livada, I. Koronakis, C. Georgakis, A. Argiriou, D.N. Assimakopoulos, On the impact of urban climate on the energy consumption of buildings, Sol. Energy 70 (3) (2001) 201–216, https://doi.org/10.1016/S0038-092X(00)00095-5.
[5] L. Allen, F. Lindberg, C.S.B. Grimmond, Global to city scale urban anthropogenic heat flux: model and variability, Int. J. Climatol. 31 (13) (2011) 1990–2005, https://doi.org/10.1002/joc.2210.
[6] F. Chen, X. Yang, J. Wu, Simulation of the urban climate in a Chinese megacity with spatially heterogeneous anthropogenic heat data, J. Geophys. Res.: Atmosphere 121 (10) (2016) 5193–5212, https://doi.org/10.1002/2015JD024642.

[7] C. Yu, D. Hu, S. Wang, S. Chen, Y. Wang, Estimation of anthropogenic heat flux and its coupling analysis with urban building characteristics – a case study of typical cities in the Yangtze River Delta, China, Sci. Total Environ. 774 (2021) 145805, https://doi.org/10.1016/j.scitotenv.2021.145805.

[8] R. Sun, Y. Wang, L. Chen, A distributed model for quantifying temporal-spatial patterns of anthropogenic heat based on energy consumption, J. Clean. Prod. 170 (2018) 601–609, https://doi.org/10.1016/j.jclepro.2017.09.153.

[9] D.J. Sailor, A review of methods for estimating anthropogenic heat and moisture emissions in the urban environment, Int. J. Climatol. 31 (2) (2011) 189–199, https://doi.org/10.1002/joc.2106.

[10] D.J. Sailor, M. Georgescu, J.M. Milne, M.A. Hart, Development of a national anthropogenic heating database with an extrapolation for international cities, Atmos. Environ. 118 (2015) 7–18, https://doi.org/10.1016/j.atmosenv.2015.07.016.

[11] C. Smith, S. Lindley, G. Levermore, Estimating spatial and temporal patterns of urban anthropogenic heat fluxes for UK cities: the case of Manchester, Theor. Appl. Climatol. 98 (1) (2009) 19–35, https://doi.org/10.1007/s00704-008-0086-5.

[12] M. Iamarino, S. Beevers, C.S.B. Grimmond, High-resolution (space, time) anthropogenic heat emissions: London 1970–2025, Int. J. Climatol. 32 (11) (2012) 1754–1767, https://doi.org/10.1002/joc.2390.

[13] W.T.L. Chow, F. Salamanca, M. Georgescu, A. Mahalov, J.M. Milne, B.L. Ruddell, A multi-method and multi-scale approach for estimating city-wide anthropogenic heat fluxes, Atmos. Environ. 99 (2014) 64–76, https://doi.org/10.1016/j.atmosenv.2014.09.053.

[14] S.I. Bohnenstengel, I. Hamilton, M. Davies, S.E. Belcher, Impact of anthropogenic heat emissions on London's temperatures, Q. J. R. Meteorol. Soc. 140 (679) (2014) 687–698, https://doi.org/10.1002/qj.2144.

[15] D. Li, E. Bou-Zeid, Synergistic interactions between urban heat islands and heat waves: the impact in cities is larger than the sum of its parts, Journal of Applied Meteorology and Climatology 52 (9) (2013) 2051–2064, https://doi.org/10.1175/JAMC-D-13-02.1.

[16] J. Yang, E. Bou-Zeid, Should cities embrace their heat islands as shields from extreme cold? Journal of Applied Meteorology and Climatology 57 (6) (2018) 1309–1320, https://doi.org/10.1175/JAMC-D-17-0265.1.

[17] W. Nie, B.F. Zaitchik, G. Ni, T. Sun, Impacts of anthropogenic heat on summertime rainfall in Beijing, J. Hydrometeorol. 18 (3) (2017) 693–712, https://doi.org/10.1175/JHM-D-16-0173.1.

[18] A. Block, K. Keuler, E. Schaller, Impacts of anthropogenic heat on regional climate patterns, Geophys. Res. Lett. 31 (12) (2004), https://doi.org/10.1029/2004GL019852.

[19] H. Fan, D.J. Sailor, Modeling the impacts of anthropogenic heating on the urban climate of Philadelphia: a comparison of implementations in two PBL schemes, Atmos. Environ. 39 (1) (2005) 73–84, https://doi.org/10.1016/j.atmosenv.2004.09.031.

[20] J. Yang, E. Bou-Zeid, Scale dependence of the benefits and efficiency of green and cool roofs, Landsc. Urban Plann. 185 (2019) 127–140.

[21] A.K.L. Quah, M. Roth, Diurnal and weekly variation of anthropogenic heat emissions in a tropical city, Singapore, Atmos. Environ. 46 (2012) 92–103, https://doi.org/10.1016/j.atmosenv.2011.10.015.

[22] M.J. Ferreira, A.P. de Oliveira, J. Soares, Anthropogenic heat in the city of São Paulo, Brazil, Theor. Appl. Climatol. 104 (1) (2011) 43–56, https://doi.org/10.1007/s00704-010-0322-7.

[23] G. Pigeon, D. Legain, P. Durand, V. Masson, Anthropogenic heat release in an old European agglomeration (Toulouse, France), Int. J. Climatol. 27 (14) (2007) 1969–1981, https://doi.org/10.1002/joc.1530.

[24] B. Yang, X. Yang, L.R. Leung, S. Zhong, Y. Qian, C. Zhao, J. Qi, Modeling the impacts of urbanization on summer thermal comfort: the role of urban land use and anthropogenic heat, J. Geophys. Res.: Atmosphere 124 (13) (2019) 6681–6697, https://doi.org/10.1029/2018JD029829.

[25] R. Zhu, M.S. Wong, É. Guilbert, P.-W. Chan, Understanding heat patterns produced by vehicular flows in urban areas, Sci. Rep. 7 (1) (2017) 16309, https://doi.org/10.1038/s41598-017-15869-6.

[26] V.K. Singh, J.A. Acero, A. Martilli, Evaluation of the Impact of Anthropogenic Heat Emissions Generated from Road Transportation and Power Plants on the UHI Intensity of Singapore, 500, Technical Report Cooling Singapore, 2020, https://doi.org/10.3929/ETHZ-B-000452434.

[27] International Energy Agency, World Energy Outlook 2019, IEA, 2019. https://www.iea.org/reports/world-energy-outlook-2019.

[28] International Energy Agency, Global EV Outlook 2020, IEA, 2020. https://www.iea.org/reports/global-ev-outlook-2020.

[29] F.N.D. Ribeiro, A.S. Umezaki, J.B. Chiquetto, I. Santos, P.G. Machado, R. M. Miranda, P.S. Almeida, A.F. Simões, D. Mouette, A.R. Leichsenring, H.M. Ueno, Impact of different transportation planning scenarios on air pollutants, greenhouse gases and heat emission abatement, Sci. Total Environ. 781 (2021) 146708, https://doi.org/10.1016/j.scitotenv.2021.146708.

[30] X. Chen, S.-J. Jeong, Shifting the urban heat island clock in a megacity: a case study of Hong Kong, Environ. Res. Lett. 13 (1) (2018), 014014, https://doi.org/10.1088/1748-9326/aa95fb.

[31] M. Cai, Y. Shi, C. Ren, Developing a high-resolution emission inventory tool for low-carbon city management using hybrid method – a pilot test in high-density Hong Kong, Energy Build. 226 (2020) 110376, https://doi.org/10.1016/j.enbuild.2020.110376.

[32] J. Song, B. Huang, J.S. Kim, J. Wen, R. Li, Fine-scale mapping of an evidence-based heat health risk index for high-density cities: Hong Kong as a case study, Sci. Total Environ. 718 (2020) 137226, https://doi.org/10.1016/j.scitotenv.2020.137226.

[33] Y. Wang, Y. Li, Y. Xue, A. Martilli, J. Shen, P.W. Chan, City-scale morphological influence on diurnal urban air temperature, Build. Environ. 169 (2020) 106527, https://doi.org/10.1016/j.buildenv.2019.106527.

[34] Y. Zheng, C. Ren, Y. Xu, R. Wang, J. Ho, K. Lau, E. Ng, GIS-based mapping of Local Climate Zone in the high-density city of Hong Kong, Urban Climate 24 (2018) 419–448, https://doi.org/10.1016/j.uclim.2017.05.008.

[35] I.D. Stewart, T.R. Oke, Local climate zones for urban temperature studies, Bull. Am. Meteorol. Soc. 93 (12) (2012) 1879–1900, https://doi.org/10.1175/BAMS-D-11-00019.1.

[36] W.C. Skamarock, J.B. Klemp, J. Dudhia, D.O. Gill, D. Barker, M.G. Duda, J. G. Powers, *A Description of the Advanced Research WRF Version 3* (No. NCAR/TN-475+STR), University Corporation for Atmospheric Research, 2008, https://doi.org/10.5065/D68S4MVH.

[37] H. Kusaka, H. Kondo, Y. Kikegawa, F. Kimura, A simple single-layer urban canopy model for atmospheric models: comparison with multi-layer and slab models, Boundary-Layer Meteorol. 101 (3) (2001) 329–358, https://doi.org/10.1023/A:1019207923078.

[38] Z.H. Wang, E. Bou-Zeid, J.A. Smith, A coupled energy transport and hydrological model for urban canopies evaluated using a wireless sensor network, Q. J. R. Meteorol. Soc. 139 (675) (2013) 1643–1657.

[39] J. Yang, Z.H. Wang, F. Chen, S. Miao, M. Tewari, J.A. Voogt, S. Myint, Enhancing hydrologic modelling in the coupled Weather Research and Forecasting–urban modelling system, Boundary-Layer Meteorol. 155 (1) (2015) 87–109, https://doi.org/10.1007/s10546-014-9991-6.

[40] E.S. Krayenhoff, A.M. Broadbent, L. Zhao, M. Georgescu, A. Middel, J.A. Voogt, A. Martilli, D.J. Sailor, E. Erell, Cooling hot cities: a systematic and critical review of the numerical modelling literature, Environ. Res. Lett. 16 (5) (2021), 053007, https://doi.org/10.1088/1748-9326/abdcf1.

[41] S.Y. Hong, J.O.J. Lim, The WRF single-moment 6-class microphysics scheme (WSM6), Asia-Pacific Journal of Atmospheric Sciences 42 (2) (2006) 129–151.

[42] J. Dudhia, Numerical study of convection observed during the winter monsoon experiment using a mesoscale two-dimensional model, J. Atmos. Sci. 46 (20) (1989) 3077–3107.

[43] E.J. Mlawer, S.J. Taubman, P.D. Brown, M.J. Iacono, S.A. Clough, Radiative transfer for inhomogeneous atmospheres: RRTM, a validated correlated-k model for the longwave, J. Geophys. Res.: Atmosphere 102 (D14) (1997) 16663–16682, https://doi.org/10.1029/97JD00237.

[44] Z.I. Janjić, The step-mountain eta coordinate model: further developments of the convection, viscous sublayer, and turbulence closure schemes, Mon. Weather Rev. 122 (5) (1994) 927–945.

[45] Y. Noh, W.G. Cheon, S.Y. Hong, S. Raasch, Improvement of the K-profile model for the planetary boundary layer based on large eddy simulation data, Boundary-Layer Meteorol. 107 (2) (2003) 401–427, https://doi.org/10.1023/A:1022146015946.

[46] F. Chen, J. Dudhia, Coupling an advanced land surface-hydrology model with the Penn State-NCAR MM5 modeling system. Part I. Model implementation and sensitivity, Mon. Weather Rev. (2001) 569–585.

[47] C. Ren, M. Cai, X. Li, L. Zhang, R. Wang, Y. Xu, E. Ng, Assessment of local climate zone classification maps of cities in China and feasible refinements, Sci. Rep. 9 (1) (2019) 1–11, https://doi.org/10.1038/s41598-019-55444-9.

[48] B.A. Johnson, S.E. Jozdani, Local Climate Zone (LCZ) map accuracy assessments should account for land cover physical characteristics that affect the local thermal environment, Rem. Sens. 11 (20) (2019) 2420, https://doi.org/10.3390/rs11202420.

[49] Y. Wang, Y. Li, S.D. Sabatino, A. Martilli, P.W. Chan, Effects of anthropogenic heat due to air-conditioning systems on an extreme high temperature event in Hong Kong, Environ. Res. Lett. 13 (3) (2018), 034015, https://doi.org/10.1088/1748-9326/aaa848.

[50] N.E. Theeuwes, G.J. Steeneveld, R.J. Ronda, B.G. Heusinkveld, L. W. A. van Hove, A.A.M. Holtslag, Seasonal dependence of the urban heat island on the street canyon aspect ratio, Q. J. R. Meteorol. Soc. 140 (684) (2014) 2197–2210, https://doi.org/10.1002/qj.2289.

[51] M. García-Díez, J. Fernández, L. Fita, C. Yagüe, Seasonal dependence of WRF model biases and sensitivity to PBL schemes over Europe, Q. J. R. Meteorol. Soc. 139 (671) (2013) 501–514, https://doi.org/10.1002/qj.1976.

[52] Y. Wang, S.D. Sabatino, A. Martilli, Y. Li, M.S. Wong, E. Gutiérrez, P.W. Chan, Impact of land surface heterogeneity on urban heat island circulation and sea-land breeze circulation in Hong Kong, J. Geophys. Res.: Atmosphere 122 (8) (2017) 4332–4352, https://doi.org/10.1002/2017JD026702.

[53] M. Yu, X. Chen, J. Yang, S. Miao, A new perspective on evaluating high-resolution urban climate simulation with urban canopy parameters, Urban Climate 38 (2021) 100919, https://doi.org/10.1016/j.uclim.2021.100919.

[54] Q. Li, J. Yang, L. Yang, Impact of urban roughness representation on regional hydrometeorology: an idealized study, J. Geophys. Res.: Atmosphere 126 (4) (2021), e2020JD033812, https://doi.org/10.1029/2020JD033812.

[55] H. Li, Y. Zhou, X. Wang, X. Zhou, H. Zhang, S. Sodoudi, Quantifying urban heat island intensity and its physical mechanism using WRF/UCM, Sci. Total Environ. 650 (2019) 3110–3119, https://doi.org/10.1016/j.scitotenv.2018.10.025.

[56] N. Zhang, X. Wang, Y. Chen, W. Dai, X. Wang, Numerical simulations on influence of urban land cover expansion and anthropogenic heat release on urban meteorological environment in Pearl River Delta, Theor. Appl. Climatol. 126 (3) (2016) 469–479, https://doi.org/10.1007/s00704-015-1601-0.

[57] X. Li, N.C. Lau, T.C. Lee, An observational study of the diurnal variation of precipitation over Hong Kong and the underlying processes, Journal of Applied Meteorology and Climatology 57 (6) (2018) 1385–1402, https://doi.org/10.1175/JAMC-D-17-0320.1.

[58] Y. Zhou, H. Guan, C. Huang, L. Fan, S. Gharib, O. Batelaan, C. Simmons, Sea breeze cooling capacity and its influencing factors in a coastal city, Build. Environ. 166 (2019) 106408, https://doi.org/10.1016/j.buildenv.2019.106408.
[59] C. Yuan, A.S. Adelia, S. Mei, W. He, X.-X. Li, L. Norford, Mitigating intensity of urban heat island by better understanding on urban morphology and anthropogenic heat dispersion, Build. Environ. 176 (2020) 106876, https://doi.org/10.1016/j.buildenv.2020.106876.
[60] J.M. Feng, Y.L. Wang, Z.G. Ma, Y.H. Liu, Simulating the regional impacts of urbanization and anthropogenic heat release on climate across China, J. Clim. 25 (20) (2012) 7187–7203, https://doi.org/10.1175/JCLI-D-11-00333.1.
[61] Transport Department, Monthly Traffic and Transport Digest, 2020. https://www.td.gov.hk/en/transport_in_hong_kong/transport_figures/monthly_traffic_and_transport_digest/2020/202012/index.html.
[62] C. Yau, Hong Kong to power ahead with electric vehicle plans, environment chief says, SCMP, 2021. https://www.scmp.com/news/hong-kong/transport/article/3124911/hong-kong-needs-plan-green-future-and-help-citys-mechanics.
[63] Y. Takane, Y. Kikegawa, M. Hara, C.S.B. Grimmond, Urban warming and future air-conditioning use in an Asian megacity: importance of positive feedback, Npj Climate and Atmospheric Science 2 (1) (2019) 1–11, https://doi.org/10.1038/s41612-019-0096-2.
[64] G. Molnár, A. Kovács, T. Gál, How does anthropogenic heating affect the thermal environment in a medium-sized Central European city? A case study in Szeged, Hungary, Urban Climate 34 (2020) 100673, https://doi.org/10.1016/j.uclim.2020.100673.
[65] J. Yang, L. Hu, C. Wang, Population dynamics modify urban residents' exposure to extreme temperatures across the United States, Science Advances 5 (12) (2019), eaay3452, https://doi.org/10.1126/sciadv.aay3452.